Supplementary Information: 'Contrasting controls on microzooplankton grazing and viral infection of microbial prey'

David Talmy, Stephen J. Beckett, Darcy A.A. Taniguchi,

Adam B. Zhang, Joshua S. Weitz, and Mick J. Follows

February 27, 2019

Contents

Appendices

A Appendix A: Encounter model derivation

Here, we outline in detail the assumptions of our biophysical model of encounter, in Equations 5 and 6 in the main text.

A.1 Encounter by swimming

We assume that encounter depends on predator detection radius (r_{detect}) and prey particle radius r_{prey}, as well as the average swimming velocity of predators and their prey (u_{pred} and u_{prey}, respectively). The modeled encounter kernel, following Evans (1989), is:

$$\rho_z = \pi(r_{detect} + r_{prey})^2(u_{pred}^2 + u_{prey}^2)^{1/2}. \tag{S1}$$

Intuition for the functional form in Equation S1 is gained by first considering the special case when prey are stationary, and $u_{prey} = 0$:

$$\pi(r_{detect} + r_{prey})^2 u_{pred}. \tag{S2}$$

In Equation S2, we assume the detection area for predators to encounter their prey is simply a circle with radius r_{detect}+r_{prey}. The volume of water swept by the predator per unit time is the detection area, multiplied by the predator swimming speed, u_{pred} (Kiørboe, 2008).

The form allowing for prey swimming (Equation S1) assumes predators and prey are clouds of particles moving in random directions, with Gaussian velocity distributions. The relative velocities also follow a Gaussian distribution with modal velocity $(u_{pred}^2 + u_{prey}^2)^{1/2}$ (Evans 1989).

A.2 Encounter by diffusion

Consider predator and prey particles with radius r_{pred} and r_{prey}, respectively. If predator and prey have diffusivity D_{pred} and D_{prey}, respectively, then the encounter due to both predator and

prey diffusion, is:

$$\rho_v = 4\pi(D_{pred} + D_{prey})(r_{pred} + r_{prey}). \tag{S3}$$

Equation S3 is a classic result derived by Smoluchowski (1917) and Chandrasekhar (1943), and has been used in ecology to understand predator-prey interactions (Weitz and Levin, 2006).

To intuit the mechanism underlying diffusive predator-prey encounter, consider first the special case when the prey are stationary, with $D_{prey} = 0$. We assume that the flow of non-motile predators, P_d, toward the static host cell follows Fick's first law of diffusion. The total flow, F, is equal to the diffusive flux, $D\frac{dP_d}{dr}$, multiplied by the surface area of the host (Kiørboe, 2008):

$$F = D\frac{dP_d}{dr}4\pi r_{prey}^2, \tag{S4}$$

where D_{pred} is the predator diffusivity constant. By rearranging Equation S4 and integrating from the surface (r_0) of the sphere to infinity

$$F\int_{r_0}^{\infty}\frac{1}{r^2}dr = \int_{P_{d,0}}^{P_{d,\infty}} 4\pi D dP_d, \tag{S5}$$

we find that the flow of predators toward the cell surface is equal to the concentration gradient of predators far from the cell, $P_{d,\infty}$, and the cell surface $P_{d,0}$, multiplied by the cell surface area, and the size-dependent diffusivity constant, D:

$$F = 4\pi D_{pred} r_{prey}(P_{d,\infty} - P_{d,0}). \tag{S6}$$

If we assume that the predator concentration at the surface of the sphere is approximately 0, then the flow is simply (Murray and Jackson, 1992):

$$4\pi D_{pred} r_{prey} P_{d,\infty}. \tag{S7}$$

The predator diffusivity D_{pred} is a function of its size, r_{pred}, and is related to temperature in Kelvin T, medium viscosity ψ, and the Boltzmann constant K (Einstein, 1905):

$$D_{pred} = \frac{KT}{6\pi\psi r_{pred}}. \tag{S8}$$

We see from Equation S8 that molecular diffusivity declines asymptotically to zero for larger predators. Thus, larger predators should have increasingly diminished encounter with host cells.

B Appendix B: Sensitivity studies

Here, we explore the general behaviour of the model in Equations 5 and 6 paying close attention to assumptions regarding prey size and effects of Brownian motion, predator and prey motility, and predator detection volume.

B.1 Sensitivity to prey size

In Figure S1, we show the size dependence of Brownian motion and motility, accounting also for the effects of prey size. Prey size has contrasting effects on encounter kernel of motile and diffusive predators, but does not change meaningfully the prediction that per-capita encounter kernel of diffusive predators decreases with size, and per-capita encounter kernel of motile predators increases with size. The lighter dashed line in Figure S1 is encounter kernel with a 0.5μm equivalent spherical radius prey, which falls toward the lower limit of bacterial size range (Figure 1a). The lighter solid line is for a prey item with a 2μm equivalent spherical radius, which falls toward the upper limit of bacteria in Figure 1a. The difference between the lighter dashed and solid line suggests that predators that depend on diffusive transport are likely to have a higher rate of encounter with large prey than with small prey. Larger prey present a larger target area for predators following a random walk, which is reflected in the linear dependence of Equation S3 on prey radius. In Figure S1, the darker dashed and solid lines are encounter kernels of individual swimming predators for 0.5μm and 2μm prey items, respectively. When swimming predators are small, the dark solid-green line is higher than the dashed line, and predators are predicted to encounter more large prey than small prey. Our model (Equation S2) assumes en-

counter kernel scales with the square of both the predator and the prey radius. For this reason, as motile predators become significantly larger than their prey, the effect of prey size diminishes.

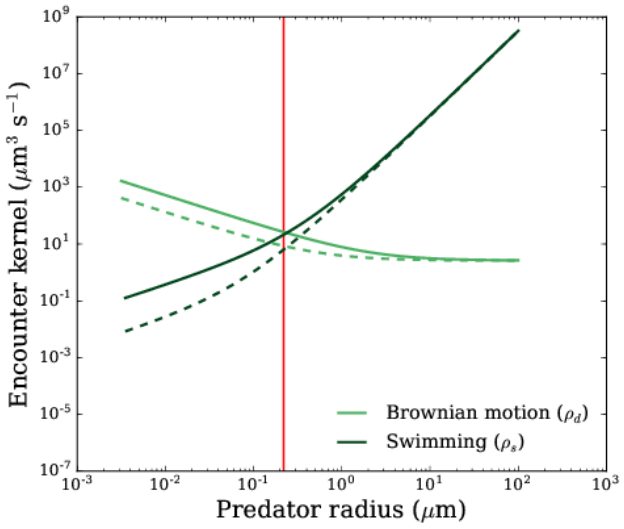

Figure S1: Theoretical encounter parameterizations for predators that move by Brownian motion and swimming. Equations S9 and S10 were used to predict encounter, separating effects of swimming (ρ_z, light green lines) from Brownian motion (ρ_v, dark green lines). Prey motion was neglected by setting u_{prey} and D_{prey} equal to zero in all cases. Dashed and solid lines are for 0.5 and 2 μm prey, respectively. For Brownian motion there is a sharp decline with predator radius due to diminishing effect of diffusion with size. Swimming has the opposite relation to predator size, with large motile predators expected to encounter more prey because they sweep a larger volume of water and swim faster (Table 2, main text). The vertical red line demarcates two domains: a small size domain where predator movement by Brownian motion is most effective, and a large size domain where and movement by swimming is most effective.

B.2 Sensitivity to prey motion

We now explore the generality of our predictions. We ask specifically: Does the predator size threshold, marked by the vertical red line in Figure S1, vary significantly if we also account for effects of prey motility and diffusion? We return to the full parameterizations presented in Equation 4, separating out encounter by a purely diffusive predator (ρ_v) from encounter by a predator that only swims for prey (ρ_z):

$$\rho_z = \underbrace{\pi(r_{prey} + r_{detect})^2 (u_{pred}^2 + u_{prey}^2)^{1/2}}_{\text{predator and prey swimming}} + \underbrace{4\pi D_{prey}(r_{pred} + r_{prey})}_{\text{prey diffusion}} \tag{S9}$$

$$\rho_v = \underbrace{\pi(r_{prey} + r_{pred})^2 u_{prey}}_{\text{prey swimming}} + \underbrace{4\pi(D_{pred} + D_{prey})(r_{pred} + r_{prey})}_{\text{predator and prey diffusion}}. \tag{S10}$$

Note that Equations S9 and S10 are identical to Equations 5 and 6 in the main text, and are repeated here for convenience. Figure S2a shows encouner kernel predictions of Equations S9 and S10, allowing prey swimming velocity to vary over the range 1-100μm s^{-1} (Milo and Phillips 2016). The blue lines show encounter kernel prediction for motile predators, and the red lines show encounter kernel of predators transported via Brownian motion. For smaller predators, encounter due to Brownian motion is higher than encounter due to swimming, but for larger predators, the opposite is true. Thus, when prey swimming is accounted for with Equations S9 and S10, smaller predators should still diffuse, and larger predators should still swim.

In Figure S2a, darker shades correspond to faster prey swimming, which enhances encounter kernel for predators that transport via both swimming, and Brownian motion. For each separate prey swimming velocity, the curves in Figure S2a have a unique predator size at which they intersect. By visual inspection, we see that the family of curves intersect approximately within the size range 0.04-0.2μm; a range toward the large end of known marine viruses (Figure 1a). Thus, even when we allow prey to swim, smaller predators have higher encounter rates from diffusion, and larger predators have higher encounter rates from swimming. The boundary marking the size at which predators should transition from Brownian motion to swimming,

coincides with the size of the largest (currently) known viruses. Does this size range change when we also account for prey diffusion? Effects of prey diffusion can be explored in a realistic range, by altering prey size in Equations S9 and S10, and assuming the same size dependence of diffusion as in Equation S8.

We determined the predator size when encounter by Brownian motion is equal to encounter by swimming, for many combinations of prey swimming velocity, and size. The prey size range explored (0.3-2 μm equivalent spherical radius) corresponds approximately to the bacteria size range depicted in Figure 1. For each prey size and swimming velocity, the predator size at which encounter by Brownian motion matches encounter by motility is shown in Figure S2b. In general, the cutoff is pushed toward smaller predator sizes for faster prey swimming, and larger sizes. The threshold predator radius contoured in Figure S2b varies approximately within the range 0.03-0.2μm, still qualitatively consistent with the size range of the largest (currently) known viruses, shown in Figure 1a. The prediction of a biophysical limit on encounter kernels of microbial predators does not change substantially when we also consider prey motility and Brownian motion.

B.2.1 Predator swimming and detection distance

The relations in Figure 2 in the main text make assumptions about the dependence of predator detection distance and swimming speed on predator size. Specifically, both detection distance and swimming speed were assumed to scale linearly with predator radius (Table 2, main text). Does the biophysical prediction of a limit on the size of microbial predators change substantially if we explore an uncertainty range in these paramerizations?

In Figure S2c, we show encounter kernel predictions of Equation S9 (blue lines), and S10 (red lines) when the predator detection factor (number of predator body lengths sensed), is varied within the range 2-30. Darker shades correspond to higher detection factors, and predictably, greater detection distance tends to enhance encounter kernels for all motile predators. Once again, smaller predators should still diffuse, and larger predators should still swim. This time

the family of curves intersect approximately within the predator size range 0.03-0.1μm, again similar to the largest known viruses (Figure 1a). What if uncertainty in the size dependence of swimming speed is also accounted for?

In Figure S2d, we show the predator size at which the encounter kernels predicted by Equations S9 and S10 intersect, allowing a wide range of both detection, and swimming speed scaling factors. The swimming uncertainty range covers a 95% confidence interval provided by linear regression of predator swimming speed with predator radius (Hansen et al., 1997, Table 2, main text). Due to the quadratic scaling with predator size, there is a stronger effect of detection scaling factor than swimming detection factor, with steeper scaling between size and detection distance pushing the predator size threshold toward smaller sizes (Figure S2c). In general, the range of size thresholds predicted by the theory is qualitatively consistent with the size range of the largest viruses shown in Figure 1a. Biophysical limits on microbial predator encounter kernels do not vary significantly when uncertainty in predator swimming and detection distance are accounted for.

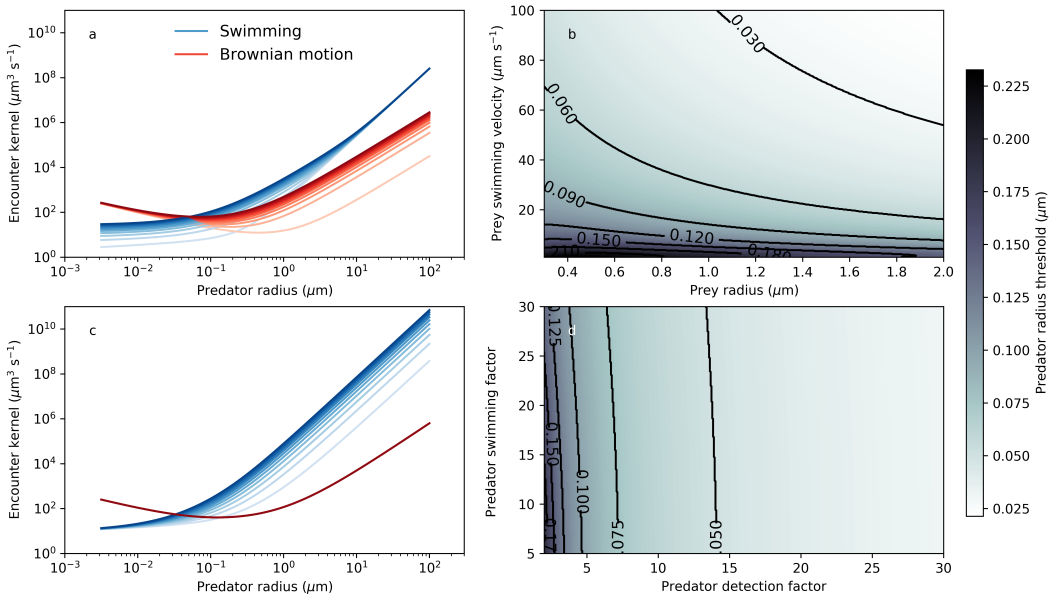

Figure S2: Size dependence of predator encounter kernels when prey motility and Brownian motion are also considered, and parameter uncertainty is explored. Equations S9 and S10 were used to predict encounter kernels for motile predators (blue lines), and diffusive predators (red lines), respectively. a) The relationship of encounter kernel with predator size; different lines correspond to prey swimming at speeds evenly spaced within the range 1-100μm s^{-1}, and darker shades correspond to faster prey swimming. b) Predator size at which the family of curves in panel (a) intersect, this time exploring a range in both predator size and swimming speed. c) Each line allows a different predator detection distance, spread evenly in the range 2-20 body lengths per individual predator. Darker shades correspond to greater predator detection factor. d) Predator size at which the family of curves in panel (c) intersect, this time exploring sensitivity to predator detection factor, and the size dependence of swimming velocity. The predator size marking the boundary between effective transport by diffusion and Brownian motion consistently falls within a size range slightly less than the largest viruses ($\sim$0.2-0.7μm equivalent spherical radius, Figure 1).

C Appendix C: Adsorption dataset

A literature search was conducted to collate adsorption data that could be compared to biophysical estimates. The search was made by searching for adsorption and bacterial host names. Information on host sizes, virus sizes and adsorption parameters was collected. However, not all information was necessarily available in the primary literature. In some cases the adsorption rate was not directly stated in the primary literature, but an adsorption curve was plotted. We digitized these curves to calculate slopes and divided these by the initial concentrations of bacteria to calculate adsorption rates. In cases where the viral size was not available we first searched the online Phages catalogue collated by the Félix d'Hérelle Reference Centre for Bacterial Viruses (https://www.phage.ulaval.ca/en/phages-catalog/) and where possible estimated virus size from electron microscopy images. If no image was available we attempted to find a reference genome size for the virus and used the following empirical formula to estimate viral radius:

$$log_{10}\left(\text{Viral radius (nm) }\right) = [1.01219 \pm 0.03928] + [0.27173 \pm 0.02231] log_{10}\left(\text{Viral genome length (kbp)}\right) \tag{S11}$$

where $\pm$ is the reported standard error. This empirical relationship was derived from 39 observations within our dataset where both viral radius and genome size were available. This relationship has an adjusted $R^2 = 0.795$ and p-value $< 1.635 \times 10^{-14}$. Previous work has suggested a strong relationship between genome size and physical size in viruses with similar scaling factors (Cui et al., 2014, Jover et al., 2014).

In total our dataset collation from the literature includes 90 measured adsorption rates. We were able to estimate viral radius for 76/90 adsorption rates and both viral and host radius for 74/90 adsorption rates.

Literature Cited

Chandrasekhar, S., 1943. Statistical problems in physics and astronomy. Rev. Mod. Phys. 15, 1–89.

Cui, J., Schlub, T. E., Holmes, E. C., 2014. An allometric relationship between the genome length and virion volume of viruses. J. Virol. 88, 6403–6410.

Einstein, A., 1905. Über die von der molekularkinetischen Theorie der Wärme geforderte Bewegung von in ruhenden Flüssigkeiten suspendierten Teilchen. Ann. Phys. 322, 549–560.

Evans, G. T., 1989. The encounter speed of moving predator and prey. J. Plankton Res. 11, 415–417.

Hansen, P., Bjornsen, P., Hansen, B., 1997. Zooplankton grazing and growth: Scaling within the 2-2,000-micrometer body size range. Limnol. Oceanogr. 42 (4), 687–704.

Jover, L. F., Effler, T. C., Buchan, A., Wilhelm, S. W., Weitz, J. S., 2014. The elemental composition of virus particles: implications for marine biogeochemical cycles. Nat. Rev. Microbiol. 12, 519–528.

Kiørboe, T., 2008. A mechanistic approach to plankton ecology. Princeton University Press.

Milo, R., Phillips, R., 2016. Cell biology by the numbers. Garland Science.

Murray, A. G., Jackson, G. A., 1992. Viral dynamics: a model of the effects of size , shape, motion and abundance of single-celled planktonic organisms and other particles. Mar. Ecol. Prog. Ser. 89, 103–116.

Smoluchowski, M. V., 1917. Mathematical theory of the kinetics of the coagulation of colloidal solutions. Zeitschrift für Phys. Chemie 92, 129–168.

Weitz, J. S., Levin, S. A., 2006. Size and scaling of predator-prey dynamics. Ecol. Lett. 9, 548–557.